

REMOTE SENSING TECHNOLOGIES IN POST-DISASTER DAMAGE ASSESSMENT

FUMIO YAMAZAKI

Department of Urban Environment Systems, Chiba University

1-33 Yayoi-cho, Inage-ku, Chiba 263-8522, Japan

MASASHI MATSUOKA

National Institute of Advanced Industrial Science and Technology (AIST)

1-1-1 Umezono, Tsukuba, Ibaraki 305-8568, Japan

This paper highlights the recent applications of remote sensing technologies in post-disaster damage assessment, especially in the 2004 Indian Ocean tsunami and the 2006 Central Java earthquake. After the 2004 Indian Ocean tsunami, satellite images which captured the affected areas before and after the event were fully employed in field investigations and in tsunami damage mapping. Since the affected areas are vast, moderate resolution satellite images were quite effective in change detection due to the tsunami. Using high-resolution optical satellite images acquired before and after the 2006 Central Java earthquake, the areas of building damage were extracted based on pixel-based and object-based land cover classifications and their accuracy was compared with visual inspection results. In the Central Java earthquake, ALOS/PALSAR captured a SAR image of the affected area one day after the event as well as pre-event times. Taking the difference of the pre-event correlation and the pre-and-post event correlation, the areas affected by the earthquake were also identified. From these examples, the use of proper satellite imagery is suggested considering the area to cover, sensor type, spatial resolution, satellite's retake time etc., in post-disaster damage assessment.

INTRODUCTION

In the recent few years, large-scale earthquakes and tsunamis brought tremendous damages to urban and rural areas in the world, especially in Asia. It is also pointed out that rapid expansion of urban areas in developing countries has made the areas more vulnerable to various natural disasters. Thus, damage assessments before and after disasters have attracted significant attentions among researchers and practitioners of disaster management. Recent advancements in remote sensing and its application technologies made it possible to use remotely sensed imagery data for assessing vulnerability of an area and for capturing the distribution of damages due to disasters.

To obtain the pre- and post-event spatial information on built and natural environments, several methods exist, such as field survey, airborne remote sensing, and satellite remote

sensing. Because of its capacity to cover a vast area in one acquisition time, satellite remote sensing has been a very powerful tool to monitor the condition of the earth surface. High-resolution satellite imagery, which has become available in the last few years, made satellite remote sensing more useful in disaster management since even the damage status of individual buildings and infrastructures can be identified without visiting the sites of disasters. The present authors have applied the images from QuickBird, the highest resolution commercial optical satellite, to obtain the damage status of individual buildings due to the 2003 Boumerdes, Algeria, earthquake (Yamazaki et al. 2004) and the 2004 Bam, Iran, earthquake (Yamazaki et al. 2005a). The recent accumulation of pre-disaster images make post-disaster images more valuable since change (damage) detection can be carried out using them.

Synthetic Aperture Radar (SAR) is another attractive tool in disaster management because SAR images can be obtained without being affected by weather condition. The present authors have applied SAR intensity images to identify the areas suffered from the collapse of buildings due to earthquakes (Matsuoka and Yamazaki 2004). The change of backscattered echo from severely damaged areas was found to be a useful index to estimate the damage extent and distribution.

In this paper, the applications of satellite imagery to post-disaster damage assessment are demonstrated for the 2004 Indian Ocean tsunami and the 2006 Central Java earthquake. The pre- and post-event satellite images are employed as base-maps for field damage survey together with GPS, and they are used in visual and automated damage detection.

THE 2004 INDIAN OCEAN TSUNAMI IN SOUTH THAILAND

Tsunami and field survey in Thailand

A moment-magnitude 9.0 earthquake struck the area off the western coast of northern Sumatra Island on 26 December 2004. The magnitude is registered as the fourth among the earthquakes worldwide after 1900. This gigantic earthquake triggered massive tsunamis, which inundated coastal areas in countries all around the Indian Ocean rim – from Indonesia to East Africa. Tsunami related deaths have been reported in 11 countries, including Indonesia, Sri Lanka, India, Thailand, Malaysia, Myanmar, Maldives, Bangladesh, Somalia, Tanzania and Kenya. The death toll including missing is approximately 280,000 according to United Nations and governments (Relief Web 2005).

In Thailand, the provinces facing Andaman Sea, notably, Phang-Nga, Phuket, and Krabi, were attacked by repeated tsunamis. The death toll in Thailand reached 5,395 and 2,932 people were listed as missing as of 09 March 2005. Nearly half of those confirmed deaths, and half of those missing were foreign tourists who were spending their holiday season in the resort areas.

As the scale of this tsunami disaster became unveiled, the present authors have decided to form an international survey team to gather geo-referenced tsunami inundation and damage information with the enhanced use of satellite images and GPS. A similar joint survey team supported by Earthquake Disaster Mitigation Research Center (EDM), NIED, Japan, and the Multidisciplinary Center for Earthquake Engineering Research (MCEER), USA, was formed

after the 1999 Kocaeli, Turkey, earthquake for the first time (Eguchi et al. 2000, EDM 2000). The joint reconnaissance survey was also conducted after the 2004 Mid-Niigata, Japan, earthquake. It was almost impossible to cover the large tsunami-affected areas by a small group. Thailand was selected as our primary survey area because of existing research



Figure 1. (a) Members of the field survey team and (b) video shooting with three videos synchronized with GPS

collaboration and accessibility to the sites at an early stage. Geo-Informatics and Space Technology Development Agency (GISTDA), Thailand, provided various satellite images for this joint survey and a visually inspected tsunami inundation map (Vibulsreth et al. 2005).

Figure 1(a) shows the members of the international survey team. The team was formed by Chiba University (Japan: F. Yamazaki), EDM (Japan: M. Matsuoka), ImageCat Inc./MCEER (USA: S. Ghosh), Asian Institute of Technology (Thailand: P. Warnitchai), GISTDA (Thailand: S. Polngam and S. Lawawirojwong), and Japan International Cooperation Agency (Japan: M. Honzawa). The primary objective of our survey is to gather geo-referenced tsunami inundation and damage information, and hence we brought several digital video cameras and digital still cameras. Figure 1(b) shows a scene of geo-referenced video shooting using three video cameras. The field survey was carried out from 8 to 11 January 2005, covering hard-hit areas, e.g. Khao Lak, Phuket Island, Phi Phi Island. Please refer the survey reports in Ghosh et al. (2005) and Yamazaki et al. (2005b).

Figure 2 shows the post-tsunami Ikonos images of Khao Lak and the photos taken during the field survey. Blue dots in Ikonos images are the location of geo-referenced photo shooting. Figure 2(a) is Ikonos image of Phakarang cape area with 1 m resolution, (b) is the photo of devastated Bamboo Orchid Resort on Phakarang cape, (c) shows a car thrown on the roof by tsunami. If we enlarge the Ikonos image, several black pixels corresponding to this car can be identified. Figure 2(d) is Ikonos image of mid Khao Lak area near a weather station, (e) is a collapsed bridge by the tsunami near the weather station, and (f) shows destroyed cottages in a resort. Figure 2(g) shows Nang Thong Beach area in lower Khao Lak, and Figures 2(h) and (i) are photos taken in Similana Resort, which was devastated by the tsunami of about 5 m high.

Panoramic VIEWS: GPS synchronized multiple video shooting

VIEWS (Visualizing the Impacts of Earthquakes With Satellites) has been developed by ImageCat, Inc. with the financial support from MCEER. VIEWS is a notebook-based system, which integrates GPS-registered digital video footage, digital photographs and observations with high-resolution satellite imagery, collected before and after a disaster (Adams et al. 2004).



Figure 2: Post-tsunami IKONOS image of Khao Lak and photos taken during the field survey. (a) Phakarang cape area, (b) devastated Bamboo Orchid Resort, (c) a car on the roof, (d) mid Khao Lak area near Weather station, (e) a collapsed bridge by tsunami, (f) destroyed cottages in a resort, (g) Nang Thong beach area in lower Khao Lak, (h) & (i) Similana Resort devastated by tsunami

VIEWS was previously used in reconnaissance activities following the 2003 Bam, Iran, earthquake, the 2004 Hurricanes Charley and Ivan that hit the Mexico Gulf coast of USA, and the 2004 Mid-Niigata, Japan, earthquake.

In this tsunami survey in Thailand, the field-based damage assessment was conducted using VIEWS. These ground-based observations can be later used to validate damage characteristics identified on satellite imagery. It is envisioned that such perishable data will be invaluable for future research in evaluating damage from tsunami hazards. We brought several video cameras in our field survey in Thailand. Thus, a new data collection approach was

adopted (Figure 1(b)) by deploying three video cameras that simultaneously captured footage for three directions (front, left, and right) in some heavily affected areas. This streamlined the video collection process and provided a wider view of the area. We named this new system as “Panoramic-VIEWS”.

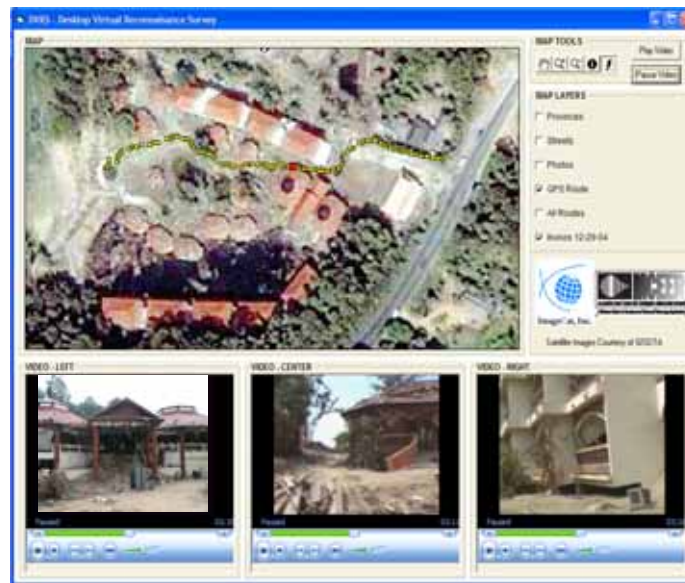


Figure 3. Screen shot from the virtual reconnaissance system, showing satellite imagery, GPS readings, video footage from three video cameras collected in Khao Lak, Thailand (Ghosh et al. 2005)

In order to integrate, share, visualize, and ultimately analyze post-disaster reconnaissance field data collected using VIEWS, MCEER funded the development of tandem internet- and desktop-based “virtual reconnaissance systems” (Ghosh et al. 2005). Figure 3 shows a screen shot from the virtual reconnaissance system, showing satellite imagery (Ikonos on 2004/12/29) with GPS readings and video footage from three video cameras collected in Khao Lak. By selecting a GPS point, users can view corresponding video footage and scroll the photographic archive in the adjacent windows.

Tsunami inundation mapping using Terra-ASTER Images

In the Indian Ocean tsunami disaster, various satellites observed the affected areas after the tsunami, and some of them have acquired images before the tsunami. ASTER (Advanced Spaceborne Thermal Emission and Reflection Radiometer) is one of the sensors on board Terra satellite (Yamaguchi et al. 1998). The visible and near-infrared radiometer of ASTER produces imagery of ground sampling interval of 15 m, and it has the three nadir-looking

bands and one backward-looking band for stereo scoping. Unlike other optical sensors, ASTER does not have a blue color band.

Terra-ASTER observed the hard-hit area including Khao Lak two years before and 5 days after the tsunami, as shown in Figure 4 in a false color composite: which means the

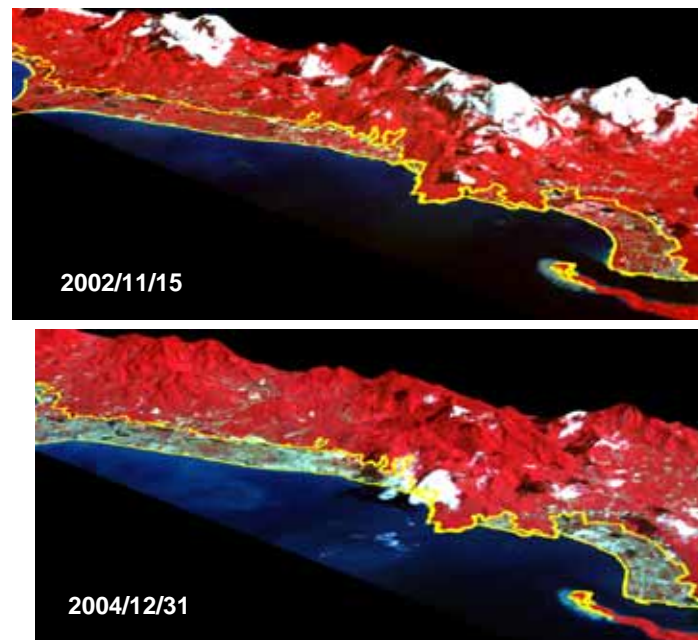


Figure 4. ASTER false color composite images of Khao Lak before (Nov. 15, 2002) and after (Dec. 31, 2004) the tsunami plotted on SRTM 90 m DEM. Yellow lines drawn over ASTER images show tsunami inundation boundary visually extracted by GISTDA.

reflectance of the near-infrared (NIR) band is assigned to the red component, that of the red (R) band to the green component, and that of the green (G) band to the blue component, respectively. The false color images are shown overlying a digital elevation model (DEM) of 90 m grid from SRTM (Shuttle Radar Topography Mission, Jet Propulsion Laboratory 2005).

Comparing these images, it could be observed that the reflectance of the near-infrared band in the affected areas became weak after the tsunami, which roughly means that, due to the tsunami, vegetation there might be removed/killed and that the land cover class might be changed to soil. This observation has also been confirmed in the field survey.

ASTER sensor can collect the data of not only visible and near-infrared bands but also a short wavelength infrared (SWIR) band. The resolution is 15 m for visible and near-infrared bands and 30 m for SWIR band. Hence, ASTER data with moderate-resolution is useful for detecting wide tsunami inundation areas quickly because red, near-infrared and short-wavelength infrared bands are considered to give the good indicators of land cover characteristics and, in fact, the normalized difference vegetation, soil and water indices have

been proposed using these three bands (Takeuchi and Yasuoka 2004). From the reflectance of the red (R), near-infrared (NIR), and short-wavelength bands (SWIR), the normalized difference vegetation (NDVI), soil (NDSI) and water (NDWI) indices can be calculated by Equations (1)-(3).

$$\text{NDVI} = (\text{NIR} - \text{R}) / (\text{NIR} + \text{R}) \quad (1)$$

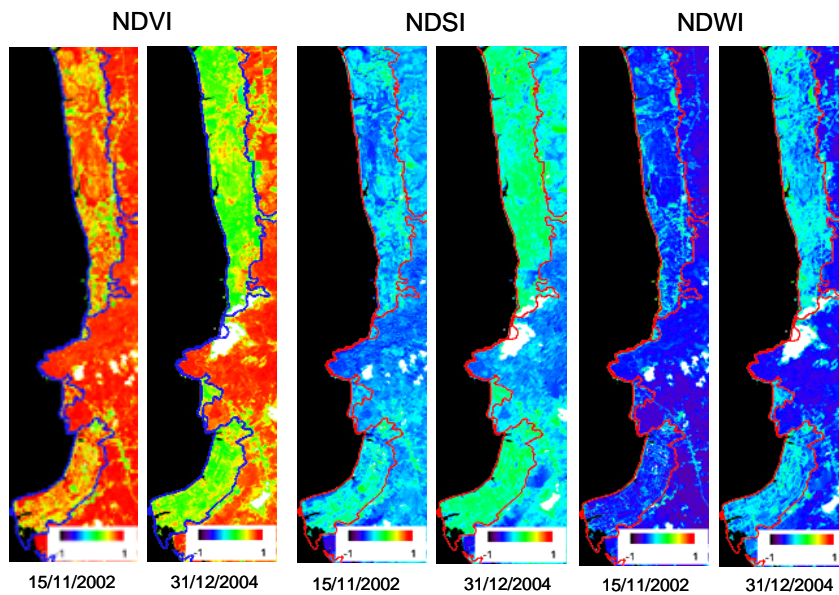


Figure 5. Computed NDVI, NDSI, and NDWI for the pre-event and post-event ASTER images.

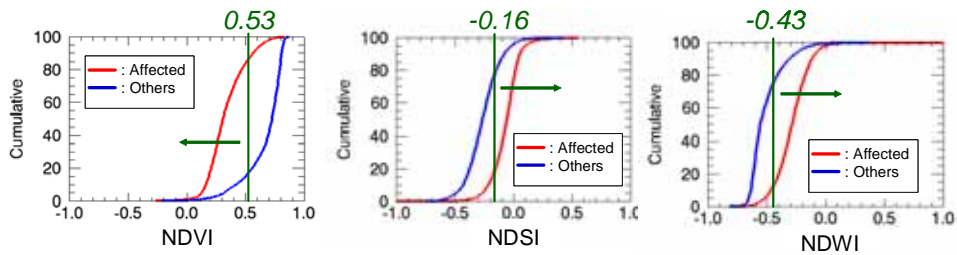


Figure 6. Cumulative frequency distributions of NDVI, NDSI, and NDWI from the data one week after the tsunami.

$$\text{NDSI} = (\text{SWIR} - \text{NIR}) / (\text{SWIR} + \text{NIR}) \quad (2)$$

$$\text{NDWI} = (\text{R} - \text{SWIR}) / (\text{R} + \text{SWIR}) \quad (3)$$

The thematic maps of NDVI, NDSI, and NDWI are shown in Figure 5. The greater NDVI becomes, the more probable the area is covered with vegetation. It is also the case with NDSI for soil and NDWI for water. The first analysis is to compare the characteristics of the three indices in the affected areas and non-affected areas using only a single post-event image, and consequently, to determine the thresholds for detection of tsunami-affected areas. This approach is applicable in the case no pre-event image exists.

The cumulative frequency distributions of NDVI, NDSI and NDWI in the affected areas and non-affected areas are plotted in Figure 6. As a result, it is observed that there are clear differences in the distributions between the two plots for each index. It is possible to determine a value where the difference between their cumulative frequency distributions is maximized as a threshold to distinguish two classes. Using this method, the thresholds to identify affected areas are 0.53 for NDVI, -0.16 for NDSI, and -0.43 for NDWI in this example. To summarize, the pixels which have NDVI value less than the threshold, and NDSI and NDWI values more than the thresholds are identified to belong to tsunami-affected areas using only the post-event image.

For moderate resolution satellite images like Terra-ASTER, pre-event images of a target area exist with high probability. Hence the comparison of pre- and post-event images is considered to be more robust than using only a post-event image. Since the significant changes of the NDVI, NDSI and NDWI values in the tsunami-affected areas are observed, it might be possible to identify tsunami-affected areas by taking the difference of the indices computed from the pre-event and post-event images.

Firstly, the pixels with NDVI less than 0.61, which is the 20 percentile of its cumulative frequency distribution in the affected areas based on the pre-event image, were excluded. In other words, we focused on the pixels showing high possibility of the existence of vegetation. For the NDSI and NDWI indices, on the contrary, only the pixels where the indices are less than -0.21 and -0.43, which are the 80 percentile of their cumulative frequency distributions based on the pre-event image, were used. Secondly, the seasonal effects were derived from the differences between the average values in the non-affected areas before and after the tsunami.

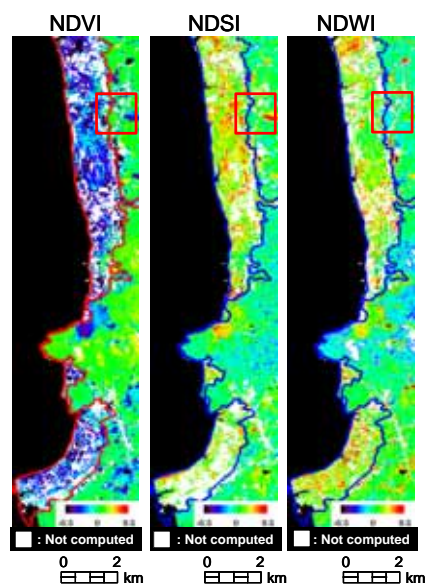


Figure 7. Differences of the three indices obtained from the pre- and post-event ASTER images.

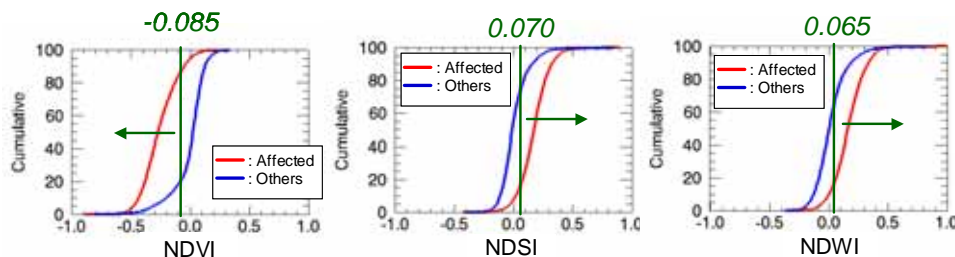


Figure 8. Cumulative frequency distributions of the differences of NDVI, NDSI, and NDWI obtained from the pre- and post-tsunami images.

After eliminating the seasonal effect, the indices' differences are illustrated in Figure 7, where white pixels were excluded from the following process.

The cumulative frequency distributions of the time differences of NDVI, NDSI, and NDWI in the affected and non-affected areas are plotted in Figure 8. Similarly to the result using only the post-event image, the thresholds for detecting tsunami-affected areas were determined. In this example, the visually extracted tsunami run-up boundary was used as the truth data. But for the case with no truth data, digital elevation models, topographic condition, and the distance from the coast line should be employed to obtain an accurate tsunami inundation map.

THE 2006 CENTRAL JAVA EARTHQUAKE

The Central Java earthquake and field survey

A strong earthquake of magnitude 6.3 struck Java Island, Indonesia, on May 27, 2006 at 5:54 am local time. The epicenter was located at 7.962°S, 110.458°E, about 25 km south-southeast of Yogyakarta with a fairly shallow focal depth, about 10 km (Figure 9). Due to this earthquake, almost 6,000 people were killed and about 38,000 people were injured. About 140,000 houses were collapsed and about 190,000 houses were heavily damaged (USGS 2006, UNOSAT 2006).

After the earthquake, various international teams conducted damage surveys of the affected area. As one of sub-teams of the research group supported by the Ministry of Education, Science, Sports and Culture (MEXT), Japanese Government, Grant-in-Aid for Special Purposes (No.1890001, 2006), the present authors visited the affected area from 26 to 30 June, 2006. The main objective of our sub-team was to gather geo-referenced ground truth data, which can be used to validate the damage detection results from satellite images. Figure 10 shows the route of the field survey. The camera icons on the map show the locations where we took geo-referenced digital photos.

Figure 11 shows typical damages observed in the field. Figure 11(a) is collapsed brick-masonry houses in a rural area. This type of total collapses of walls and roofs were seen everywhere and considered to be responsible for many casualties in this earthquake in spite of

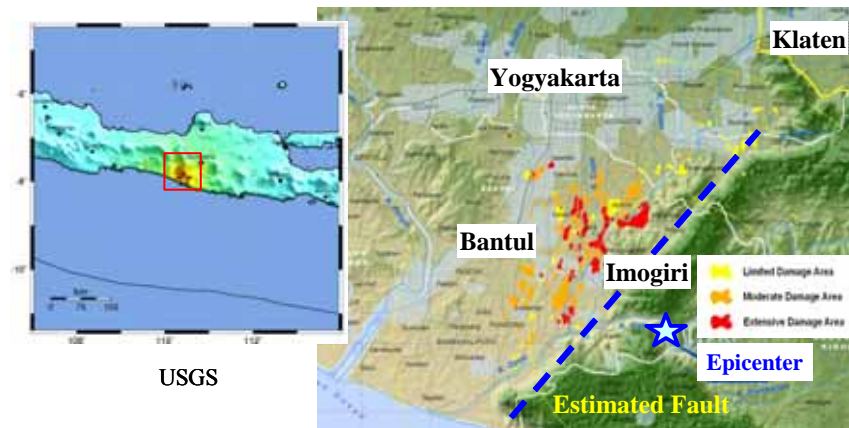


Figure 9. Epicenter of the 2006 Central Java earthquake (USGS 2006) and preliminary damage assessment map produced by UNOSAT (2006) on May 31, 2006.

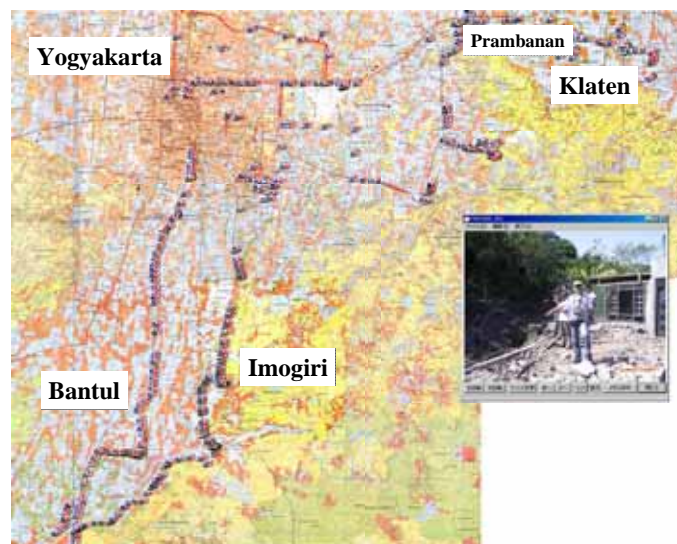


Figure 10. Field survey route by the authors. Camera icons show the locations of GPS synchronized photo shooting.

its small magnitude. Figure 11(b) shows a collapsed reinforced-concrete school building. Such severe damages to engineered buildings were seen only at limited locations. Figure 11(c) shows a large-scale landslide observed in a mountainous area. In Prambanan World Heritage, the largest Hindu temple compound in Indonesia, many big stones were fallen down from the towers as shown in Figure 11(d). The site has been closed to tourists since the earthquake and it was reported that the restoration may take a few years.



Figure 11. Typical damages seen in the field survey: (a) collapsed brick-masonry houses in a rural area, (b) a collapsed reinforced-concrete school building, (c) a large-scale landslide observed in a mountainous area, (d) stones fallen down from the towers in Prambanan temple compound.

Damage detection using QuickBird image

QuickBird has 0.6 m resolution in panchromatic mode and 2.4 m resolution in multispectral mode with 4 bands: blue, green, red, and near-infrared. A pan-sharpened image of 0.6 m resolution can be produced through combining a panchromatic image and a corresponding multispectral image. After the Java Earthquake, QuickBird captured a clear image of the affected areas on June 13, 2006. The image includes Imogiri, one of the most severely affected areas in this earthquake. For the area, a pre-event image captured on July 11, 2003 also exists. Thus a part of these images, shown in Figure 12, were used in this study.

First, a pixel-based classification was carried out based on the maximum likelihood method, the most common supervised classification method, using 8-bit four bands data. The following 8 classes: black-roof, gray-roof, red-roof, white-roof buildings, road, soil, vegetation, and shadow, were assigned for the pre-event image as the training data. For the post-event image, 7 classes: black-roof, gray-roof, red-roof buildings, debris, road, vegetation, and shadow, were assigned. White-roof building and soil classes were not used for the post-event image because they look close to the debris class and it was difficult to select their training data. The building areas obtained by the pixel-based classification are shown in Figure 13 (a) and Figure 14 (a). In these figures, the buildings with different roof-color are shown in the same color for easier understanding.

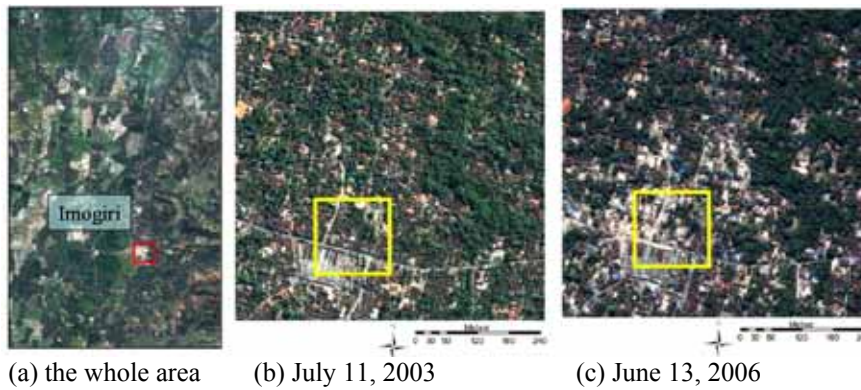
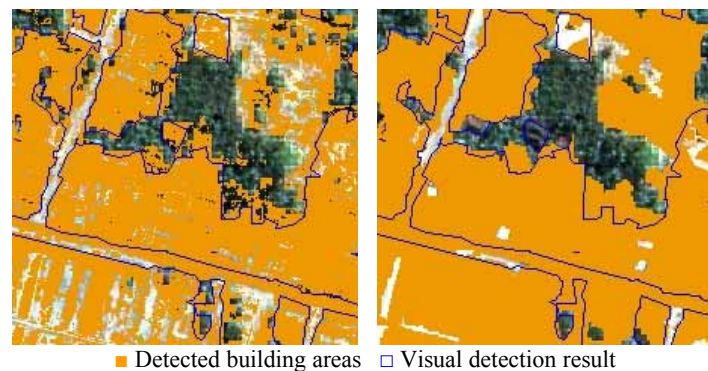


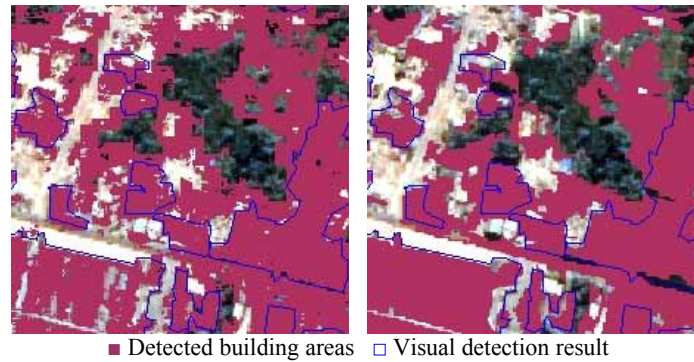
Figure 12. (a) Pan-sharpened natural color QuickBird images of Imogiri area, (b) is the pre-event image and (c) is the post-event image used in this study.



(a) Pixel-based classification (b) Object-based classification

Figure 13. Part of the pre-event image (yellow square in Figure 12 (b)) and the result of land cover classifications.

Next, an object-based classification was conducted using e-Cognition software. Image segmentation was carried out as the first step to make “objects” using the pre-event and post-event images. In e-Cognition, the segmentation process is determined by 5 parameters: *Layer Weight*, *Compact Weight*, *Smooth Weight*, *Shape Factor*, and *Scale Parameter* (Baatz et al. 2004). The most important parameter is the *Scale Parameter*, which determines the object size. The *Shape Factor* is to determine the importance level of spectral heterogeneity or shape heterogeneity in segmentation. When the shape factor moves toward 0, the spectral heterogeneity is more concerned. On the contrary, if it moves toward 0.9, the shape heterogeneity is more concerned. In further details, the spectral heterogeneity is decided by *Layer Weight*, which gives the weight for each band. The shape heterogeneity is decided by *Compact Weight* and *Smooth Weight*. The bigger the Compact Weight is, the segmented



(a) Pixel-based classification (b) Object-based classification

Figure 14. Part of the post-event image (yellow square in Figure 12 (c)) and the result of land cover classifications.

objects are in a more compact shape. Alternatively, the bigger the Smooth Weight is, the segmented objects are in a more smooth shape.

Starting from pixels, segmentation runs the merge between two objects and is terminated when an assigned condition is reached. This condition is defined based on the fusion value f , which measures the changes when merging and decided by the Layer Weight, Compact Weight, Smooth Weight, and Shape Factor. If f equals to or becomes bigger than the squared Scale Parameter, the condition is reached. Although it is difficult to decide the appropriate parameters values suitable to all land cover classes, the user can decide the suitable values to a few focused classes, e.g. building, road.

The appropriate parameters for buildings were used in this study and the image segmentation was conducted for the pre-event and post-event images. Then, the samples for all the classes were selected as the same areas in the pixel-based classification. The objects' mean values of blue, green, red, and near-infrared were used as the indices of classification and the nearest neighbor classification method was employed.

The results from the object-based classification for the pre-event and post-event images are shown in Figures 13 (b) and 14 (b), respectively. Comparing the results from the pixel-based and object-based classifications with that by visual inspection, salt-and-paper noises are seen in the pixel-based classification. Hence, it may be concluded that in this high resolution and the sizes of the target objects, the better result can be acquired by object-based classification. But in object-based classification, some road and shadow areas were misclassified to building classes because their spectral values of the sample area are similar to those of building classes. Hence even object-based classification, some classes like these are needed to remove in advance using object feature indices, e.g. length, or spatial relationships.

Damage detection using ALOS/SAR

The Advanced Land Observing Satellite (ALOS, “Daichi” in Japanese), was launched successfully on January 24, 2006, by the Japan Aerospace and Exploration Agency (JAXA). After providing first shots captured by the onboard sensors, PRISM, AVNIR-2, and PALSAR (Phased Array Type L-band Synthetic Aperture Radar), ALOS has been performing the image acquisition of natural disasters at an early stage, such as the mudslide occurred in Leyte Island, the Philippines, on February 17, 2006, the volcanic eruptions of Mt. Merapi, Indonesia, from April to May 2006, and the flood in north Thailand on May 2006.

A good quality image of the affected areas was captured by PALSAR one day after the 27 May 2006 Central Java earthquake. Fortunately, time-series pre-event PALSAR images have already been acquired and available to use in change (damage) detection because the earthquake source and the affected areas are located rather near Mt. Merapi volcano. In this study, two pre-seismic images (April 29 and May 16, 2006) and one post-seismic image (May 28, 2006) were employed for the affected areas such as Bantul and Yogyakarta regions and applied them in change detection, evaluating the difference in pre- and co-seismic correlations.

By activating the disaster charter (International Charter 1999), L-band SAR system, PALSAR (HH polarization with 9 m resolution) onboard ALOS, was operated for capturing the information on the areas damaged due to the earthquake. Figure 15 shows the backscattering intensity images of time-series PALSAR covering Yogyakarta and central Java provinces. On the next day of the earthquake, PALSAR observed the area successfully in 36.9 degree off-nadir angle (microwave transmission angle). Two pre-event images had also been obtained on April 29 and May 16, 2006 with 34.3 and 30.8 degree off-nadir angles, respectively. Using these images, the variation of the correlation coefficient was calculated and the effects of signal noise and stationary temporal changes were evaluated. The

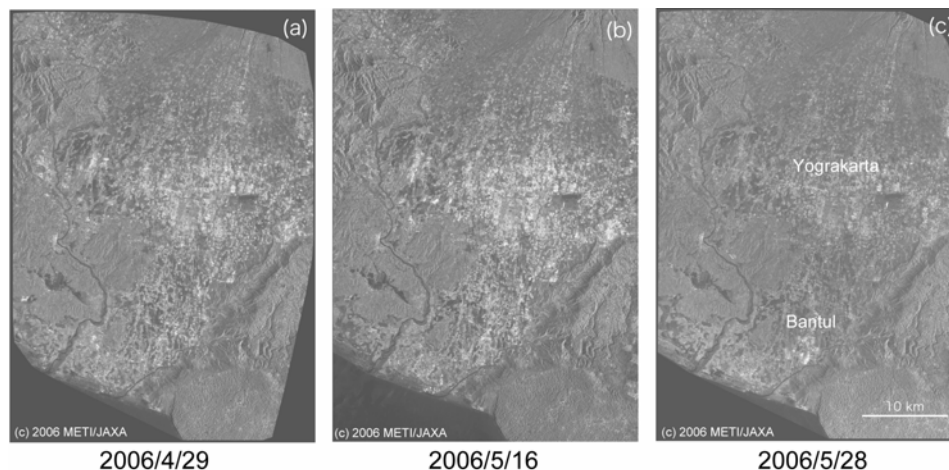


Figure 15. Backscattering intensity images of Yogyakarta area from ALOS/PALSAR before and after the 27 May 2006 Central Java earthquake.

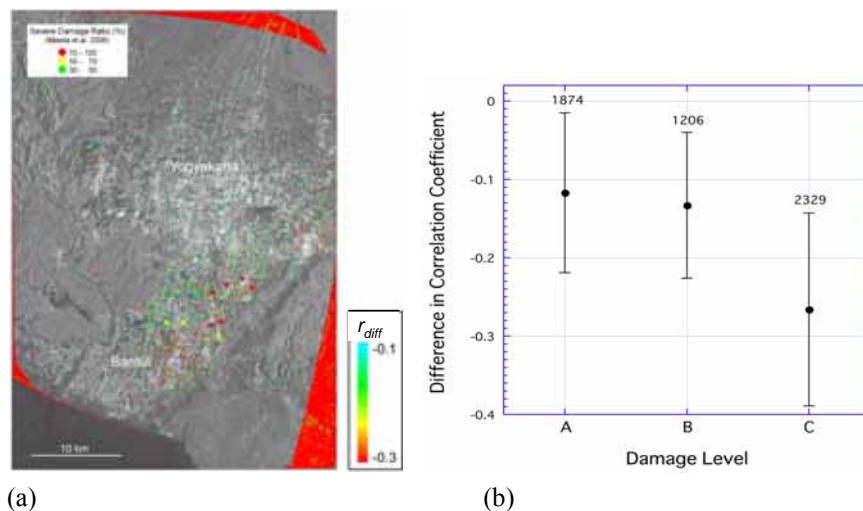


Figure 16. (a) Distribution of the difference, r_{diff} , between correlation coefficients derived from ALOS/PALSAR imagery, plotted on the post-earthquake backscattering intensity image. Areas with extremely negative r_{diff} values at the edge of the image are errors due to image co-registration. The colored circles indicate the building damage ratio surveyed by Maeda et al. (2006). (b) Relationship between the building damage level and the difference between correlation coefficients, r_{diff} . The damage levels were classified as A, B or C, corresponding to damage ratios of 30-50%, 50-70% and 70-100%, respectively.

distribution of the difference, r_{diff} , between the r_{bb} value of the two pre-event images and the r_{ab} of the pre- and post-event images plotted on PALSAR intensity image is shown in Figure 16 (a). To focus on built-up areas, the decorrelated areas (correlation coefficient less than 0.8) from the pre-event pair were excluded from the analysis in advance. In Bantul, the lower r_{diff} areas distribute from southwest to northeast, showing good agreement to the estimated damaged areas (see Figure 9) by visual interpretation from high-resolution satellite images (UNOSAT 2006).

A Japanese field survey team carried out an intensive building damage investigation around schools and obtained the ratio of severely damaged buildings in a 500 m radius from a school (Maeda et al. 2006). In Figure 16 (a), twelve investigated areas (colored-circles classified by the severely damaged ratio) are also plotted on the r_{diff} distribution.

For a quantitative analysis, we selected pixels within the investigated circles in the field survey and calculated the average and standard deviation of r_{diff} value in each damage level. The damage levels classified into A, B, and C, correspond to the severely damaged ratio of 30-50, 50-70, and 70-100 %, respectively. The comparison between the building damage level and the difference in correlation coefficient, r_{diff} , is shown in Figure 16 (b). The numbers on the top of the error bars represent the counts of pixels. In the figure, as the damage level increases, the difference in the correlation coefficient is seen to decrease although the standard

deviation is quite large. The similar trend was also observed in SAR intensity images from several damaging earthquakes (Matsuoka and Yamazaki 2004, 2005).

CONCLUSIONS

The recent applications of remote sensing technologies in post-disaster damage assessment were highlighted using the satellite imagery obtained in the 2004 Indian Ocean tsunami and the 2006 Central Java earthquake, as typical examples.

After the 2004 Indian Ocean tsunami, various satellite images which captured the affected areas before and after the event were fully employed in field investigations and in tsunami damage mapping. Comparing the pre- and post-event optical images visually, tsunami affected areas were easily identified. Since the affected areas are vast, moderate resolution satellite images, e.g. Terra-ASTER, were quite effective in change detection analysis using the NDVI and other land cover indices.

After the 2006 Central Java earthquake, high-resolution optical satellite images were fully employed to extract the areas of severe building damage. In our field investigation, satellite images were used as base-maps together with GPS. Comparing the pre-and post-event QuickBird images, the areas of severe building damage were extracted based on pixel-based and object-based classifications and their accuracy was compared with visual inspection results. In the Java earthquake, ALOS/PALSAR captured a SAR image of the affected area one day after the event as well as pre-event times. Taking the difference of the pre-event correlation and the pre-and-post event correlation, the areas affected by the earthquake were also extracted in good accuracy.

In summary, satellite images can be used efficiently in post-disaster damage assessment if they are selected properly in terms of sensor type (optical or SAR), spatial resolution, satellite's retake time, and the availability of pre-event images and digital maps, etc.

ACKNOWLEDGMENTS

We would like to thank the Japan Aerospace Exploration Agency (JAXA) for providing the ALOS/PALSAR data under collaborated research. Some research outputs introduced in this paper have been produced by Mr. K. Kouchi of Nippon Koei Co., Ltd. and Mr. K. Matsuomoto of Chiba University. Their contributions are deeply appreciated.

REFERENCES

- Adams, B.J., Huyck, C.K., Mansouri, B. et al. (2004). "The Bam (Iran) earthquake of December 26, 2003: Preliminary reconnaissance using remotely sensed data and the VIEWS system", MCEER Earthquake Reconnaissance Investigation Report, 10p. <http://mceer.buffalo.edu/research/Bam/page1.asp>.
- Batz, M., Benz, U., et al. (2004). *e-Cognition user guide 4*, Definiens Imaging, 76-78.

- Earthquake Disaster Mitigation Research Center (EDM) (2000). “*Report on the Kocaeli, Turkey Earthquake of August 17, 1999, The 1999 Turkey Earthquake report*”, EDM Technical Report, No. 6, p. 67.
- Eguchi, R.T., Huyck, C.K., Houshmand, B., Mansouri, B., Shinozuka, M., Yamazaki, F., and Matsuoka, M. (2000). “*The Marmara Earthquake: A view from space, The Marmara, Turkey Earthquake of August 17, 1999: Reconnaissance report*”, Technical Report MCEER-00-0001, 151-169.
- Ghosh, S., Huyck, C.K., Adams, B.J., Eguchi, R.T., Yamazaki, F., and Matsuoka, M. (2005). “Preliminary field report: Post-tsunami urban damage survey in Thailand, using the VIEWS reconnaissance system”, <http://mceer.buffalo.edu/>
- International Charter (1999) “Space and Major Disaster”, <http://www.disasterscharter.org/>.
- Jet Propulsion Laboratory (2005). “Shuttle Radar Topography Mission (SRTM)”, <http://www2.jpl.nasa.gov/srtm/index.html>
- Maeda, M. et al. (2006). “Reconnaissance report of building damage due to the 2006 Mid Java, Indonesia Earthquake”, Ver. 2006/7/18 (in Japanese).
- Matsuoka, M. and Yamazaki, F. (2004). “Use of satellite SAR intensity imagery for detecting building areas damaged due to earthquakes”, *Earthquake Spectra*, 20 (3), 975-994.
- Matsuoka, M. and Yamazaki, F. (2005). “Building damage mapping of Iran earthquake using Envisat/ASAR intensity imagery”, *Earthquake Spectra*, 21(S1), S285-S294.
- Relief Web (2005). <http://www.reliefweb.int/rw/RWB.NSF/db900SID/EVIU-6AJJ3C?OpenDocument&rc=3&cc=tha>
- Takeuchi, W., and Yasuoka, Y. (2004). “Development of normalized vegetation, soil and water indices derived from satellite remote sensing data”, *Journal of the Japan Society of Photogrammetry and Remote Sensing*, Vol. 43, No. 6, 7-19 (in Japanese).
- UNOSAT (2006). Indonesia Maps, <http://unosat.web.cern.ch/unosat/asp/>.
- USGS (2006) URL: <http://earthquake.usgs.gov/eqcenter/eqinthenews/2006/usneb6/>
- Vibulsreth, S., Ratanasermpong, S., Polngam, S. (2005). “Tsunami disasters along the Andaman Sea, Thailand”, *Asian Journal of Geoinformatics*, Vol. 5, No. 2, 3-15.
- Yamaguchi, Y., Kahle, A.B., Pniel, M., Tsu, H., and Kawakami, T. (1998). “Overview of Advanced Spaceborne Thermal Emission and Reflection Radiometer (ASTER)”, *IEEE Transactions on Geoscience and Remote Sensing*, 36 (4), 1062-1071.
- Yamazaki, F., Kouchi, K., Matsuoka, M., Kohiyama, M., and Muraoka, N. (2004). “Damage Detection from high-resolution satellite images for the 2003 Boumerdes, Algeria Earthquake”, *Proceedings of the 13th WCEE*, CD-ROM, Paper No. 2595.
- Yamazaki, F., Yano, Y., and Matsuoka, M. (2005a). “Visual damage interpretation of buildings in Bam city using QuickBird images”, *Earthquake Spectra*, Vol. 21, No. S1, S329–S336.
- Yamazaki, F., Matsuoka, M., Warnitchai, P., Polngam, S., and Ghosh, S. (2005b). “Tsunami reconnaissance survey in Thailand using satellite images and GPS”, *Asian Journal of Geoinformatics*, Vol. 5, No. 2, 53-61.